



1 **Seasonal prediction of springtime tornado activity in the United States using**
2 **a hybrid model**

3 Authors: Matthew Graber¹, Zhuo Wang¹, & Robert J. Trapp¹

4 ¹Department of Climate, Meteorology, & Atmospheric Sciences, University of Illinois Urbana-Champaign,
5 Urbana, 61820, United States

6 Correspondence to: Zhuo Wang (zhuowang@illinois.edu)

7 **Abstract:** Tornado activity in the contiguous United States (CONUS) causes fatalities and
8 financial losses every spring, motivating attempts to skillfully predict springtime tornadoes. Such
9 predictions would facilitate decision-making and resource management for both public and
10 private stakeholders. Using ERA5 reanalysis, we identify five April-May weather regimes
11 (WRs) from 1981-2023, some of which strongly modulate tornado activity. ECMWF seasonal
12 forecasts initialized on April-1st are applied to predict WR frequency, including persistent and
13 non-persistent WRs (lasting ≥ 5 and < 5 consecutive days, respectively). The WR information are
14 incorporated into a hybrid model to predict April-May CONUS tornado activity, including
15 tornado outbreaks (days with > 10 EF-1+ tornadoes). Prediction skill is evaluated using leave-
16 one-year-out cross-validation. Predicted and observed tornado outbreak frequencies are
17 significantly correlated ($cc=0.4$). Outbreak predictions are more skillful during the positive phase
18 of the Arctic Oscillation (AO) and Pacific North American pattern (PNA), with a proportion
19 correct of 0.75 and 0.71, respectively. This implies that low-frequency climate modes can be
20 used to identify forecasts of opportunity. SSTs over the North Pacific and North Atlantic may
21 help explain the predictability of tornado activity but further work needs to be done to confirm
22 those results. Our study demonstrates the potential for skillful prediction of spring tornado
23 outbreaks using WR forecasts and should be prioritized in future work.

24 **1. Introduction**

25 Tornadoes in the contiguous United States (CONUS) result in significant losses of life and
26 property (Ashley 2007; Strader et al. 2024; NCEI 2024). From 1981-2023 there were 2833
27 tornado-related fatalities in the CONUS, accounting for $\sim 13\%$ of weather-related fatalities
28 (National Weather Service 2025). Of these tornado-related fatalities, roughly 80% are associated
29 with tornado outbreaks (TOs) (Schneider et al. 2004). Recent studies show a statistically
30 significant increasing trend of $+2.5$ TOs per decade since 1960, the majority of which occur in the
31 boreal spring (Grabner et al. 2024; Brooks et al. 2014). Given these trends of tornado activity and
32 their societal impacts, skillful seasonal predictions of springtime tornado activity would improve
33 decision-making and resource management for both public and private stakeholders. Subseasonal-
34 to-seasonal (S2S) predictability of tornado activity has been previously investigated. Deterministic
35 and probabilistic GEFS forecasts demonstrated skill in predicting tornado activity out to day 9
36 (Gensini and Tippett 2019). The Extended-Range Tornado Activity Forecast (ERTAF) project
37 (Gensini et al. 2020) produced tercile-forecasts 2-3 weeks in advance during boreal spring and
38 found predictive skill at both lead times. ERTAF emphasized the role of large-scale circulation
39 patterns in conjunction with favorable severe thunderstorm environments, such as adequate
40 convective available potential energy (CAPE) and vertical wind shear (VWS). Baggett et al. (2018)
41 developed an empirical model using MJO phases and skillfully predicted weekly severe weather
42 forecasts out 2-5 weeks in March-June. Similarly, Lepore et al. (2017) applied extended logistic
43 regression based on the winter ENSO state to predict tornadoes in March-May, and found that the
44 tornado prediction skill is higher during La Niña years compared to El Niño years. This



45 background motivates the work herein that seeks to further explore skillful season prediction of
46 tornado activity.

47 Low-frequency climate modes are important drivers of seasonal tornado activity and can serve as
48 sources of their predictability. For example, La Niña (El Niño) winters tend to coincide with more
49 (fewer) tornadoes in the winter (Cook and Schaefer 2008), and winter ENSO indices have been
50 previously linked to springtime tornadoes (Allen et al. 2015; Lepore 2017). Lee et al. (2016)
51 implied that springtime ENSO phase may be used to improve TO predictability, specifically.
52 Across the CONUS, tornado activity during La Niña years peaks in mid-April, whereas activity
53 during El Niño years peaks in late-May, when overall tornado frequency is greater than during La
54 Niña (Allen et al. 2018). Furthermore, Tippett et al. (2022) found that a positive (negative) phase
55 of the Arctic Oscillation (AO) coinciding with La Niña (El Niño) may increase (decrease) late
56 winter and early spring tornado activity. The positive AO phase in winter and early spring on its
57 own has been found associated with enhanced tornado activity (Childs et al. 2018; Niloufar et al.
58 2021; Tippett et al. 2022), while Elsner et al. (2016) found that the positive phase of the North
59 Atlantic Oscillation (NAO) is linked to a decrease in springtime tornado activity in the Southeast.
60 Additionally, the negative phase of the Pacific North American Pattern (PNA) is connected to a
61 stronger Intra-Americas low-level jet and increased springtime tornado activity in the Midwest
62 and Southeast (Munoz and Enfield 2011). Furthermore, positive sea surface temperatures (SST)
63 anomalies in the Gulf of Mexico have been associated with increased tornado activity over the
64 Southeast during the spring (Molina et al. 2016), and Chu et al. (2019) demonstrated the link
65 between TOs and SST anomalies in April via a negative PNA pattern.

66 Though low-frequency climate modes provide an avenue for understanding the predictability of
67 tornado activity, they do not fully capture the day-to-day variability of atmospheric circulation
68 patterns that drive weather. This gap can be filled by weather regimes (WRs). WRs represent a
69 finite number of equilibrium, recurring states of the atmospheric circulation (Michelangeli et al.
70 1995; Charney and DeVore 1979; Hannachi et al. 2017). Miller et al. (2020) is among the first to
71 apply WRs to tornado prediction. They constructed a hybrid prediction model for weekly tornado
72 activity in May using WRs and achieved skillful prediction out to week 3. Tippett et al. (2024)
73 explored the modulation of tornado activity using year-long WRs (Grams et al. 2017; Lee et al.
74 2023) and found statistically significant relations between tornado reports and WRs during all
75 months except June-August, with results mainly driven by years with more Pacific Ridge WR
76 days. Graber et al. (2025) identified two WRs that strongly affect the warm-season tornado
77 activity, especially TOs, and developed an empirical model using WR frequency, persistence, and
78 TD probabilities. The empirical model skillfully captures the interannual variability of both TDs
79 and TOs using WR information derived from the ERA5 reanalysis and motivate its application to
80 seasonal prediction.

81 The remainder of this paper is organized as follows. Section 2 describes the data and methodology,
82 including the hybrid model. Section 3 presents the hybrid predictions and a discussion of the
83 sources of predictability that help connect the WRs, tornado activity, and climate modes together.
84 The paper will culminate with a summary and discussion in Section 4.

85 **2. Methodology**

86 **2.1 Weather Regimes**

87 Daily 500-hPa heights (500H) from the ERA5 reanalysis (Hersbach et al. 2020) were used to
88 identify weather regimes (WRs) during April-May, the season of peak tornado activity (Graber et
89 al. 2024), from 1981-2023. The seasonal cycle, defined as the long-term mean 500H for each



90 calendar day, was removed from daily 500H. We used the WRs derived by Graber et al. (2025)
91 using the K-means clustering method for 1960-2022 April-July as the reference WR patterns, and
92 WRs were assigned by finding the reference WR pattern with the smallest Euclidean distance from
93 the daily 500H anomalies. We took this approach because K-means clustering yields slightly
94 different WR patterns in different time periods, and employing WRs during a longer time period
95 as the reference patterns improves the robustness of the results.

96 Seasonal forecasts of daily 500H anomalies from the European Centre for Medium-Range Weather
97 Forecasts (ECMWF) were used to predict April–May WR frequency from 1981-2023 (Vitart et
98 al. 2017; Copernicus Climate Change Service 2018). The 25-ensemble forecasts are initialized
99 once per month and are available on a $1^\circ \times 1^\circ$ grid. The forecasts initialized on April 1st were
100 selected to mitigate the effect of the spring-predictability barrier (Duan and Wei 2012). WRs were
101 assigned for each ensemble forecast by projecting the forecast 500H anomalies to the reference
102 WR patterns, and the resultant long-term mean WR frequencies are similar to those derived from
103 ERA5. Persistent and nonpersistent WRs are defined as WRs lasting for ≥ 5 consecutive days and
104 for < 5 consecutive days, respectively.

105 2.2 Tornado observations

106 Tornado reports during April-May 1981-2023 were obtained from the NOAA Storm Prediction
107 Center Severe Weather Database. Reports are georeferenced with time, date, and EF/F rating.
108 Tornado days (TDs) are defined as days with ≥ 1 tornadoes ranked EF/F-1 or greater, and tornado
109 outbreaks (TOs) are defined as any day with > 10 tornadoes ranked EF/F-1 or greater (Graber et al.
110 2024, 2025). EF/F-0 reports were excluded due to reporting uncertainties (Brooks et al. 2014;
111 Trapp 2013). Known biases remain in this database, which a focus on TDs rather than raw tornado
112 reports attempts to alleviate (Brooks et al. 2014; Trapp 2014; Graber et al. 2024).

113 2.3 Hybrid model

114 Following Graber et al. (2025), an empirical model was used to evaluate the seasonal prediction
115 of tornado activity:

$$116 \quad TI(t) = \sum_{i=1}^5 f(i, t)_p \times P_{i,p} + \sum_{i=1}^5 f(i, t)_{np} \times P_{i,np} \quad (1)$$

116 where P_i denotes the TD probability for each WR, which is defined as the number of TDs with
117 WR- i divided by the number of total WR- i days. The predictand tornado index for year t , $TI(t)$, is
118 computed by the seasonal count of WR- i days in year t , $f(i, t)$, multiplied by P_i . TD probabilities
119 and counts were calculated for persistent and nonpersistent WRs separately, denoted by subscripts
120 p and np , respectively. The same procedure was applied to TOs (Graber et al. 2025).

121 To evaluate tornado prediction skill, a leave-one-year-out cross-validation method was employed.
122 Specifically, 1981 was first held for testing, and $P_{i,np}$ and $P_{i,p}$ were determined using the WR
123 information derived from the ERA5 reanalysis and tornado reports during 1982-2023. The
124 seasonal WR counts from the ECMWF ensemble forecasts for 1981 were used in Eq. 1 to predict
125 the TI value in 1981. This process was repeated for each year, yielding a predicted time series of
126 TI. The TI time series for all ensemble members were averaged to form the ensemble mean TI,
127 which was standardized using z-score normalization.



128 The prediction skill was quantified using the Pearson correlation between predicted and observed
129 TI time series. Additionally, a three-tier categorical verification was used by classifying both
130 observed and predicted TI values into lower, middle, and upper terciles. A correct prediction was
131 recorded when the observed and predicted TI values fell within the same tercile for a given year.
132 The proportion correct (PC) is defined as the number of correct predictions divided by the number
133 of total predictions.

134 To assess the potential impacts of climate modes on tornado predictability, PC was calculated
135 separately for positive, negative, and neutral phases of various low-frequency climate modes (see
136 more information on climate modes in section 2.4). Significance ($p \leq 0.05$) between PC of each
137 phase and random chance (33% for three-tier verification) was determined using a Monte Carlo
138 test with 10,000 resamples.

139 **2.4 Sources of Predictability**

140 The impacts of some low-frequency climate modes on tornado activity and WR counts were
141 investigated to provide a physical basis for TD and TO predictability. Indices of ENSO (via
142 ENSO3.4), PNA, NAO, and AO were downloaded from the NOAA Climate Prediction Center
143 (2024a,b). Positive and negative phases of a climate mode are defined as the years when the
144 standardized springtime (April-May) index exceeded ± 0.9 . 0.9 was used instead of 1.0 to slightly
145 increase the sample size.

146 TD and TO probability anomalies were calculated for each climate mode phase as:

$$P_a = \frac{P_r - P_c}{P_c} \times 100\% \quad (2)$$

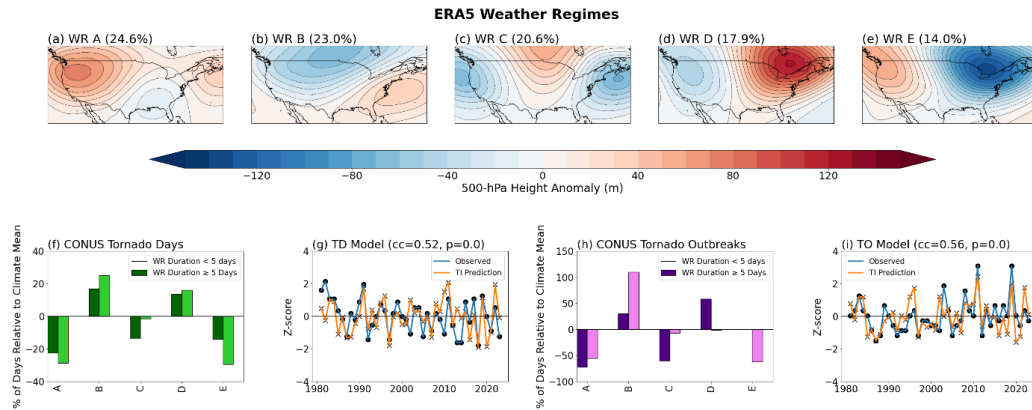
147 where the climatological mean TD probability (P_c) is defined as the total number of TDs divided
148 by the total number of days; P_r is TD probability for the given phase of the climate mode; and P_a
149 is the percentage anomaly.

150

151 **3. Results**

152 **3.1 Model Prediction**

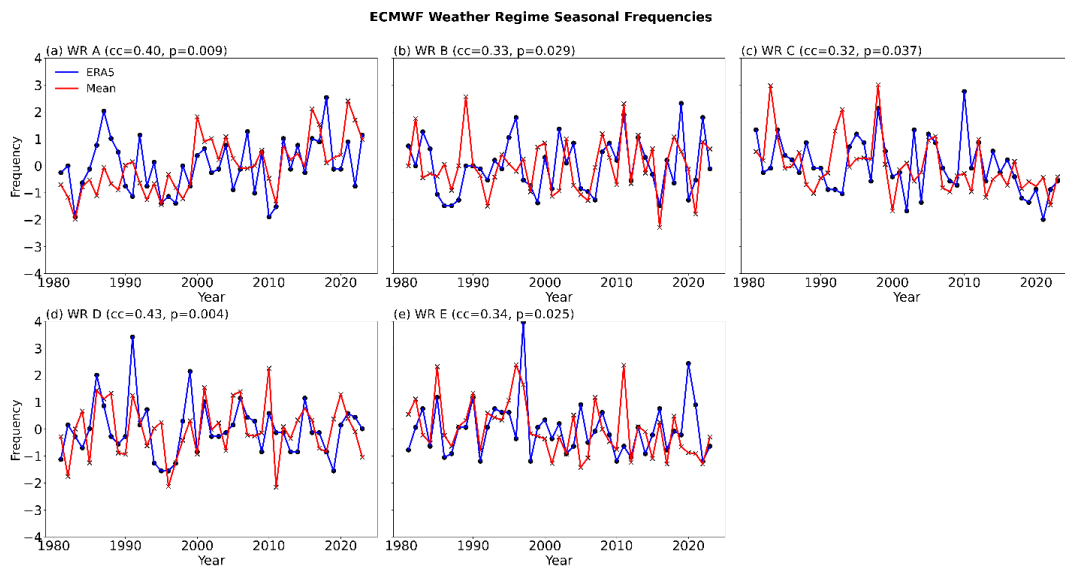
153 For completeness, the five WRs (Fig. 1a-e) are briefly described here. WR-A features anomalous
154 highs over both the eastern and western U.S. coasts. WR-B is characterized by a prevailing
155 anomalous low centered over central North America and an anomalous high over the Southeast
156 CONUS. WR-C exhibits a three-cell wave pattern with anomalous lows over both coasts. WR-D
157 and WR-E display west-east dipole patterns that nearly mirror each other. The WR spatial
158 structures closely resemble WRs in Miller et al. (2020), Zhang et al. (2024), and Lee et al. (2023).
159 Specifically, WR-A and WR-E resemble the Pacific Ridge and Alaskan Ridge regimes in Lee et
160 al. (2023), respectively, but noticeable differences exist due to differences in data processing
161 procedures and the time periods analyzed. The impacts of the WRs on tornado activity in the
162 CONUS during April-May 1981-2023 (Fig. 1f and 1h) are similar to those during April-July 1960-
163 2022 from Graber et al. (2025; their Fig. 4). WR-A is the least favorable WR for springtime tornado
164 activity, and WR-B is the most favorable. Tornado activity in WR-C and WR-E are slightly
165 unfavorable, and in WR-D is slightly favorable. The estimated TDs and TOs based on the empirical
166 model (Eq. 1) and the ERA5 during April-May 1981-2023 are significantly correlated with the
167 observed time series (Figs. 1g and 1i).



168

169 **Figure 1:** 500H anomaly patterns of WRs A-E with long-term frequency indicated in panel title (a-e). ERA5 tornado
 170 day (f) and tornado outbreak (h) CONUS probability anomalies for persistent (≥ 5 days) and nonpersistent (< 5)
 171 WRs. Time series of standardized tornado days (g) and tornado outbreak days (i) from the observation (blue) and
 172 estimation of the empirical model modeling (red). Spearman rank correlation and p-value are indicated in panels g
 173 and i.

174 Before assessing the hybrid predictions of tornado activity, we first evaluate the prediction skill of
 175 WRs by the ECMWF springtime forecasts. The ECMWF ensemble mean prediction of springtime
 176 WR counts are significantly correlated with the ERA5 springtime WR counts (Fig. 2a-e). This
 177 indicates the seasonal predictability of WRs and provides the basis for tornado prediction using
 178 the hybrid framework (i.e., Eq. 1).

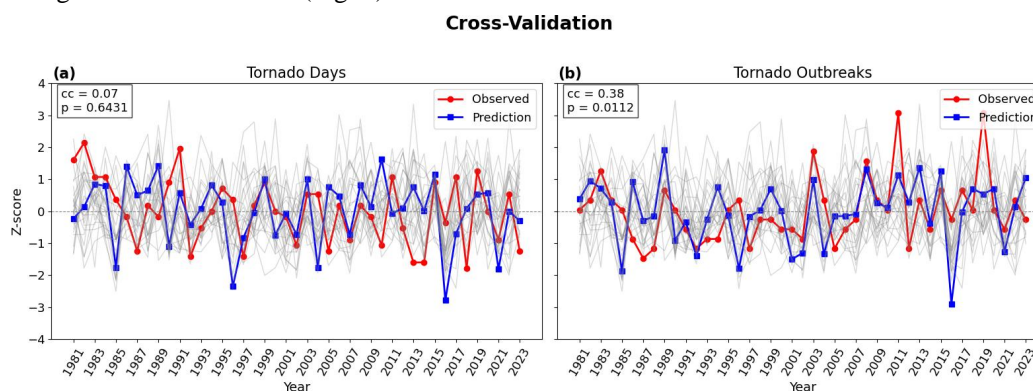


179

180 **Figure 2:** Z-score normalized ERA5 (blue) and ECMWF ensemble mean (red) springtime frequency of each WR with
 181 Spearman rank correlation and p-value indicated in each panel (a-e).



182 We assess the hybrid predictions of TDs and TOs using leave-one-year-out cross-validation
183 method (Fig. 3a-b). The hybrid prediction of TOs has a significant Pearson correlation of **0.38** with
184 the observed TO time series, while TD prediction shows no skill, with a Pearson correlation close
185 to zero. The skill contrast between the TO and TD predictions is probably because TOs usually
186 occur under strong and persistent synoptic-scale patterns (Mercer et al. 2012; Cwik et al. 2022;
187 Jiang et al. 2025; Graber et al. 2025), while some transient, weak WR days, which are not well
188 captured by the ECMWF springtime forecasts, may have strong impacts on TDs. In addition, it is
189 worth noting that the percentage anomalies of TOs associated with various WRs are generally
190 stronger than those of TDs (Fig. 1).

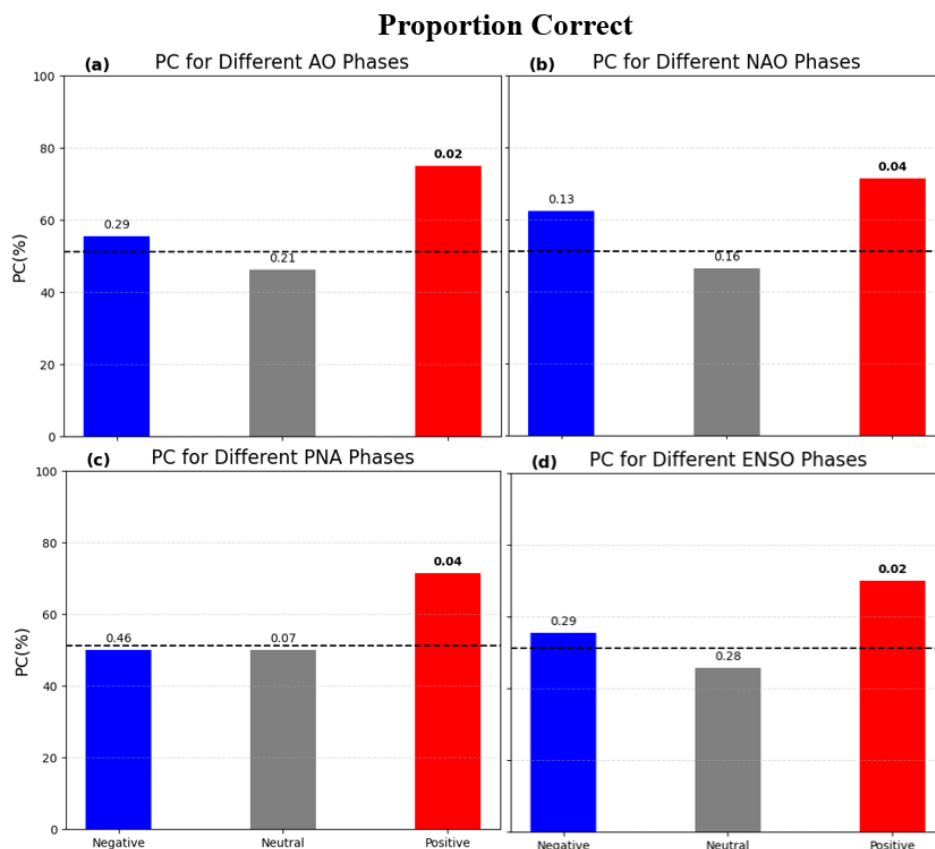


191
192

193 **Figure 3:** Standardized TDs (a) and TOs (b) time series from observation (red) and the hybrid prediction
194 (blue). Thin gray lines represent the individual ensemble prediction (grey) time series. Pearson correlations
195 (cc) and p-values (p) are shown at the upper left corner of each panel.

196 The tercile-based TO prediction indicates that the hybrid model correctly predicts **53.5%** of years.
197 Additionally, the PC is strongly modulated by some climate modes (Fig. 4). In particular, the
198 hybrid model performs significantly better during the positive phases of the AO (**75%** of correct
199 prediction), NAO (**71.4%**), PNA (**71.4%**), and ENSO (**70.0%**). PC also improves in the negative
200 phases of NAO (**62.5%**), AO (**55.6%**), and ENSO (**55.6%**), but the increases in PC are not
201 significant ($p > 0.05$). In contrast, the PC in a neutral phase is below **53.5%**. Although the PC of
202 the tercile-based TD prediction is close to random chance (**34.9%**), the hybrid model performs
203 better in +PNA years (**57.1%**, $p=0.23$) (figure not shown). This suggests that climate modes may
204 be used to identify forecasts of opportunity for springtime tornado prediction.

205 Additional cross-validation tests by leaving two-, three-, four-, and six-year out yield similar
206 results (Fig. S1). TO predictions maintain skillful across all tests, while TD predictions remain
207 unskillful.



208

209 **Figure 4:** Proportion of correct TO predictions for negative (blue), neutral (grey), and positive (red) phases
 210 of AO (a) and NAO (b), PNA (c), and ENSO (d). Numbers above the bars represent p-values using a Monte
 211 Carlo test with 10,000 resamples, and bold values represent significant ($p \leq 0.05$) differences from random
 212 chance. The dashed, horizontal line represents the overall PC (i.e., 53.5%).

213 3.2 Low-frequency climate modes as sources of Predictability

214 To investigate predictability sources for tornado activity, the relationship between tornado activity
 215 and low-frequency climate modes is examined using springtime TD and TO probability anomalies
 216 associated with the AO, NAO, PNA, and ENSO phases (Figs. 5a-h). In addition to CONUS, we
 217 examined different regions, Midwest (MW), Southern Great Plains (SGP), Southeast (SE), and
 218 Southern Great Plains (SGP). The region definitions follow Moore (2018), with exception of the
 219 SGP, which herein contains New Mexico because it has storm events similar to those in the Texas
 220 Panhandle.

221 Significantly enhanced TO probability in the CONUS and Midwest is associated with the -AO
 222 phase. TO probability is also enhanced in the SE, NGP and SGP, but the anomalies are not
 223 statistically significant. In contrast, the probability anomalies of TDs during +AO and -AO phases
 224 are much weaker and all insignificant, consistent with Tippett et al. (2022) showing a weaker
 225 tornado-AO relationship in April than in February. +AO years are characterized by an anomalous
 226 high over the southeastern CONUS and negative anomalies over the north-central CONUS (Fig.



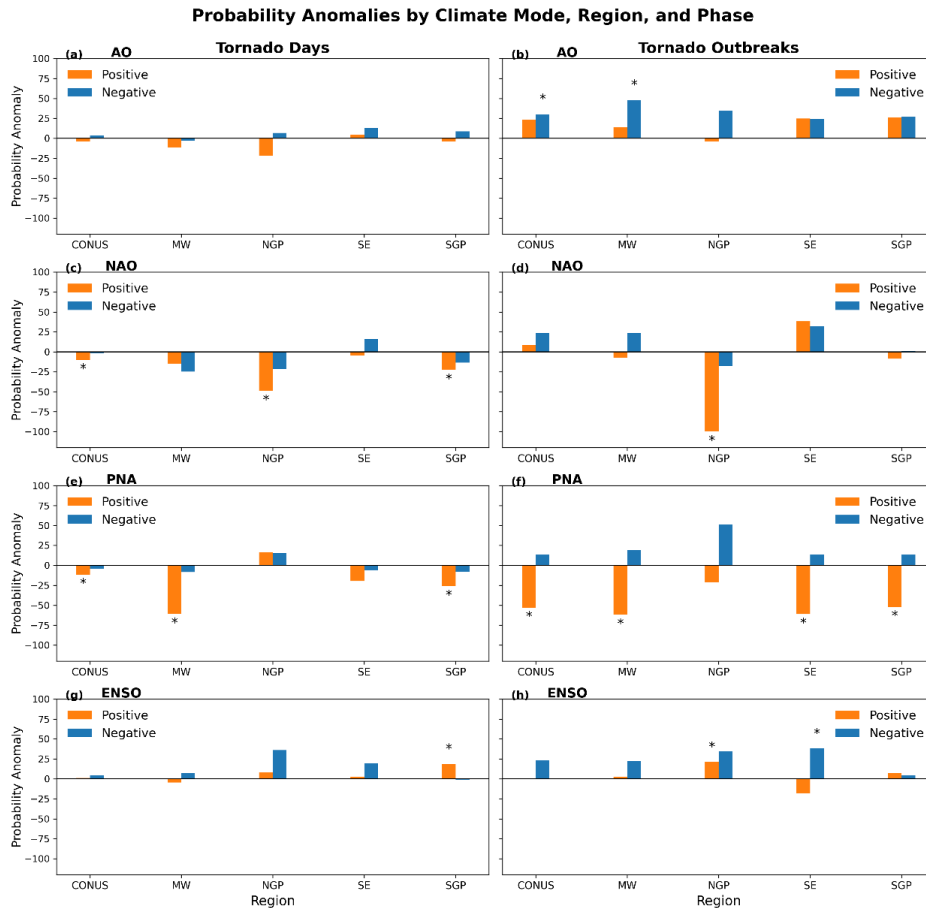
227 S2a), implying enhanced westerly flow aloft and promoting moisture and warm-air advection from
228 the Gulf of Mexico. These circulation anomalies lead to positive MUCAPE and TD probability
229 anomalies over the Southeast and SGP (Fig. S2a). In contrast, -AO years feature negative 500H
230 anomalies over the central CONUS, accompanied by anomalously positive VWS. Although
231 anomalously low MUCAPE during -AO years tends to suppresses TD probability, the enhanced
232 VWS supports anomalously positive TO probability anomalies (Sherburn et al. 2016).

233 The TD and TO probability anomalies during the NAO phases are generally consistent in sign with
234 those during AO phases, but quantitative differences exist. TD probability is reduced significantly
235 over CONUS, SGP, and NGP, and TO probability is reduced significantly over NGP during the
236 +NAO phase. +NAO years feature an anomalous 500H high over the west-central CONUS, which
237 hinders moisture and heat transport from the Gulf of Mexico. These circulation changes result in
238 anomalously low MUCAPE and TD probabilities over the SGP and NGP (Fig. S2e). Additionally,
239 anomalously low VWS over the SGP further limits tornado potential during +NAO years.
240 However, +NAO years feature an anomalous 500H high over the western Atlantic, which enhances
241 southerly flow and moisture transport into the Southeast (Zhao et al. 2025), supporting positive
242 MUCAPE anomalies (Fig. S2e) and corresponding positive TO probability anomalies in that
243 region (Fig. 5).

244 The positive PNA phase (+PNA) is unfavorable for tornado activity across the CONUS, MW,
245 SGP, and SW, particularly for TOs (Fig. 5f). +PNA years feature an anomalous 500H high over
246 the western CONUS and an anomalous 500H low over the eastern CONUS (Fig. S2c), implying
247 reduced moisture transport from the Gulf of Mexico and anomalously low VWS. These circulation
248 anomalies hinder tornado activity across the MW, SGP, and SW. Springtime PNA has become
249 more negative over time (Fig. S3), possibly explaining the increasing trend in TOs (Graber et al.
250 2024), though further work with other seasons needs to be done to confirm this.

251 TO probability is enhanced in La Nina years in various regions, although the enhancement is
252 significant only in SE. Additionally, TD probability over SGP and TO probability over NGP are
253 enhanced in El Nino years. The La Nina-tornado-activity link is largely consistent with previous
254 work (e.g., Cook and Schaefer 2008; Cook et al. 2017; Tippett et al. 2022; Allen et al. 2015; Moore
255 2019), but it is worth noting that the ENSO state in the spring time is examined here, while some
256 previous studies focus on the winter ENSO state.

257 Overall, the link between climate modes and tornado activity suggests that low-frequency climate
258 modes provide a source of predictability for springtime tornado prediction. Additionally, low-
259 frequency climate modes modulate TO probabilities more strongly than TD probabilities,
260 consistent with the stronger TO anomalies associated with WRs (Fig. 1h) and the higher predictive
261 skill of TOs (Fig. 3).



262

263 **Figure 5:** TD (left column) and TO (right column) probability anomalies by region and climate mode: AO
 264 (a-b), NAO (c-d), PNA (e-f), and ENSO (g-h). Asterisks represent significant anomalies ($p \leq 0.05$) based
 265 on a Monte Carlo test with 10,000 resamples of each regions' data.

266 The connection between climate modes and WRs is examined next to investigate whether climate
 267 modes modulate tornado activity via WRs. Figure 6 shows the frequency of WRs in different
 268 phases of low-frequency climate modes, which is defined as the number of WR days during a
 269 given phase of the climate mode divided by the total number of days in that phase. The frequency
 270 of WR-A is only ~15% during the -AO phase, while the frequency of WR-B is ~33% (Fig. 6).
 271 The increased occurrence of WR-B and decreased occurrence of WR-A in -AO years compared to
 272 the long-term mean (Fig. 1) are consistent with the positive TO probability anomalies in the
 273 CONUS and Midwest during the -AO years (Fig. 5).

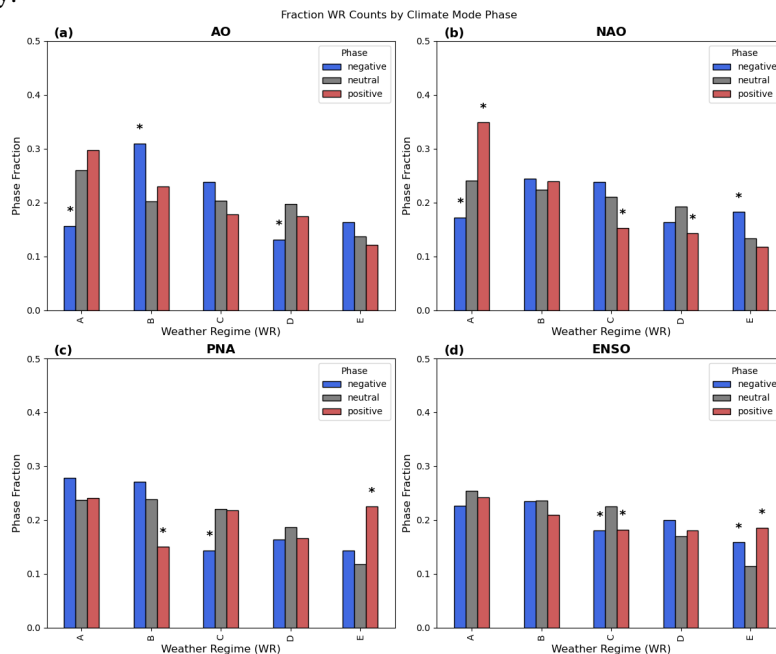
274 During +NAO years, WR-A occurs on approximately 35% of days, making it the dominant WR
 275 during this phase. This predominance of WR-A is consistent with the reduced TD probability in
 276 the CONUS, NGP, and SGP, and reduced TO probability in the NGP during NAO+ years (Fig. 6).
 277 Composite 500H anomalies for +NAO years resemble WR-A, while composite 500H anomalies for
 278 for +AO show a mix of WR-A and WR-B (Fig. S2).



279 During +PNA years, WR-B occurs on ~15% of days, whereas WR-E occurs on ~25% of days,
 280 making it the most frequent WR during this phase (Fig. 6). The reduced occurrence of WR-B and
 281 increased occurrence of WR-E are consistent with reduced TD and TO activity over CONUS,
 282 MW, and SGP during +PNA (Fig. 5). Composite 500H anomalies during +PNA years resembles
 283 WR-E, with an anomalous high over the western CONUS and an anomalous low over the eastern
 284 CONUS (Fig. S2c).

285 Neither positive nor negative phase of ENSO is associated with significant changes in WR-A or
 286 WR-B frequency. Instead, the frequency of WR-C is reduced significantly in both phases of
 287 ENSO, and WR-E occurs more frequently in the positive phase of ENSO, which is consistent with
 288 the reduced tornado activity during El Nino years reported in previous studies (Cook et al. 2017).

289 To summarize, WRs associated with increased springtime tornado activity tend to occur more
 290 frequently during the climate mode phases that favor increased tornado activity, while WRs
 291 associated with suppressed tornado activity preferentially occur during climate mode phases that
 292 are unfavorable for tornado activity. These consistent relationships provide additional confidence
 293 in the robustness of the WR-based prediction framework and help to understand tornado
 294 predictability.



295

296 **Figure 6:** WR frequencies in different phases of AO (a), NAO (b), PNA (c), and ENSO (d). An asterisks indicates
 297 that the frequency is significantly different ($p \leq 0.05$) from that during the corresponding neutral phase via a student
 298 t-test.

299 3.3 Possible role of SST

300 In addition to low-frequency climate modes, slowly-evolving SST may also serve as an important
 301 source of predictability. The connection between SSTs, large-scale circulations, and tornado
 302 activity is examined in Fig. 7. Extended Range SST (ERSST) (Huang et al. 2017) of $2^\circ \times 2^\circ$
 303 resolution is used here, and we focus on the month of April because SST signals in April are more



304 pronounced than in May based on a previous study (Chu et al. 2019) and our own analysis. In
305 addition, the analysis is done for 1960-2023 to increase the sample size. For each WR, active and
306 inactive years are identified as the years when the springtime count of the WR exceeds ± 1
307 standard deviation from the mean, and composite anomalies of SST and 500H are constructed for
308 these active and inactive years of the WR.

309 +WR-A years are characterized by an anomalous 500H high over the north-central CONUS, as
310 part of a well-defined wavetrain pattern extending from the North Pacific to southern Greenland,
311 in addition to an anomalous low over the Southeast and Gulf of Mexico. Although there are
312 coherent cold and warm SST anomalies associated with the anomalous low and high over the
313 North Pacific, respectively, the SST anomalies are not significant. Significant SST anomalies exist
314 over the North Atlantic associated with anomalous 500H high. In contrast, the -WR-A years
315 feature an anomalous low over the central CONUS, nearly opposite to the +WR years. However,
316 the anomalous circulation patterns over the North Pacific and North Atlantic are not a simple
317 mirror image to those during +WR-A years. The anomalous 500H field is characterized by an
318 elongated anomalous low over the midlatitude North Pacific and North Atlantic, reminiscent of
319 the -AO pattern. Significant SST anomalies are found over the North Pacific and North Atlantic,
320 resembling the Atlantic tripole SST pattern, which helps to maintain the NAO pattern via positive
321 air-sea interaction (Czaja and Frankignoul 2002). Consistent with this circulation, WR-A is
322 suppressed during -NAO and -AO years (Fig. 6).

323 WR-B is most favorable for tornado activity over the CONUS. Though positive SST anomalies
324 exist over the central Pacific in +WR-B years, consistent with that shown in Chu et al. (2019) for
325 April tornadoes, the anomalies are not significant. The 500H pattern over the North Atlantic is
326 reminiscent of a -AO pattern, consistent with increased WR-B occurrence during -AO (Fig. 6).
327 Significant, negative SST anomalies exist over the North Pacific in -WR-B years. The associated
328 North Pacific negative SSTs and the 500H high over Canada are reminiscent of a +PNA pattern,
329 consistent with reduced WR-B occurrence during +PNA (Fig. 6). Though insignificant, the warm
330 SST anomalies in the northern Pacific during +WR-B have been previously linked to enhanced
331 CONUS tornado activity (Zhao et al. 2025) through a weakening and eastward shift of the Aleutian
332 Low (Chu et al. 2019), which promotes enhanced southerly flow of moisture and heat from the
333 Gulf of Mexico.

334 +WR-C years feature anomalously cold SSTs in the midlatitude North Pacific and North Atlantic
335 as well as in the Gulf of Mexico. The cold SST anomalies over the Gulf of Mexico may limit
336 moisture availability (Molina et al. 2016), partially offsetting the otherwise favorable southerly
337 500H anomalies over the central US. This compensating thermodynamical and dynamical effects
338 help explain the near-climatological tornado activity during WR-C (Fig. 1f, h). In contrast, -WR-
339 C years are associated with prevailing warm SST anomalies in the North Pacific. Significant SST
340 anomalies, however, are confined to the subtropical North Atlantic and portions of the subtropical
341 eastern Pacific.

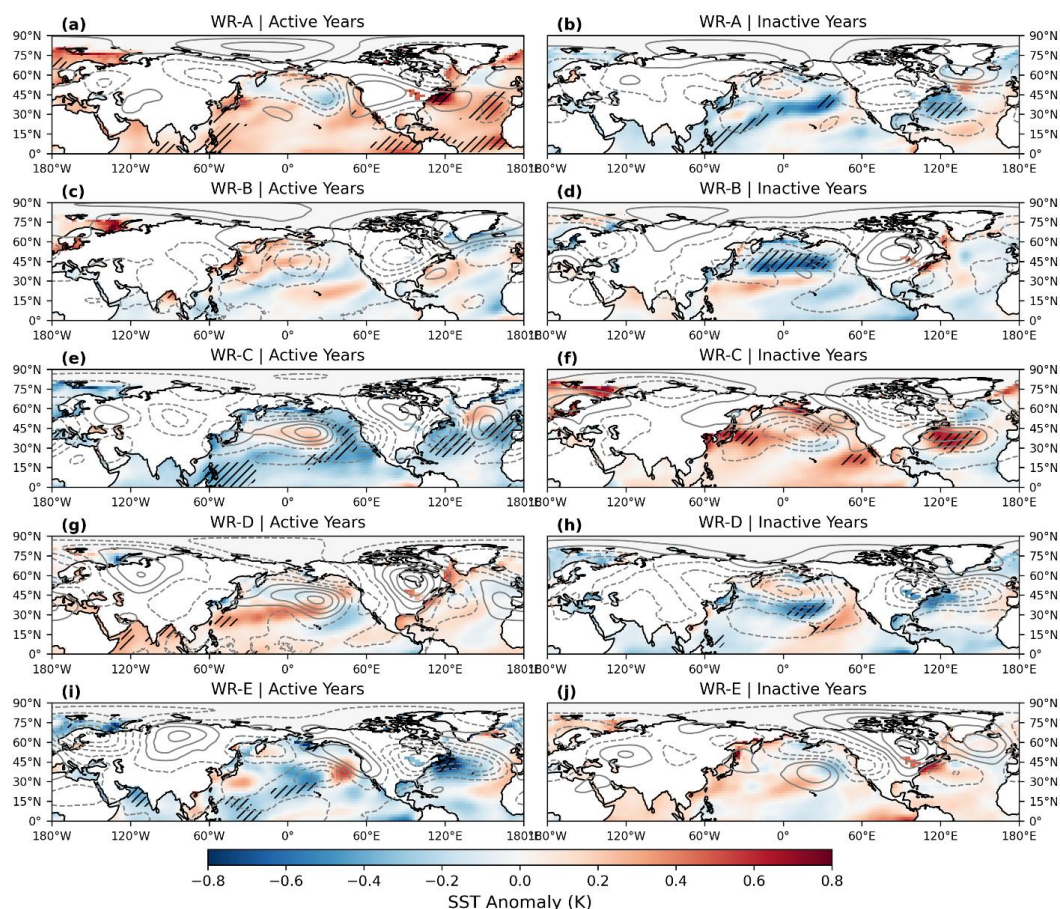
342 +WR-D and +WR-E years feature anomalously warm and cold SSTs in the Gulf of Mexico,
343 respectively, though these anomalies are not statistically significant. Over the subtropical western
344 and central North Pacific, respectively, +WR-D years exhibit significant warm SST anomalies,
345 while +WR-E years show significant cold SST anomalies. Given that WR-D and WR-E are linked
346 to enhanced and reduced TD probability, respectively (Fig. 1), this suggests that SST anomalies in
347 the subtropical Pacific may be a source of predictability for tornado activity over the CONUS.
348 However, the robustness of this relationship requires further examination given the patchy pattern



349 of the significant SST signals, and the underlying mechanisms also need to be investigated. In
350 addition, significant cold SST anomalies exist over the North Atlantic for +WR-E years,
351 suggesting cold SSTs in this region may be associated with reduced TD probabilities over the
352 CONUS.

353 Overall, Fig. 7 suggests that SST anomalies over the North Pacific and North Atlantic may help
354 explain the predictability of some WRs and thus the predictability of tornado activity within the
355 hybrid framework. However, WR-B and WR-D, which favor tornado activity over the CONUS
356 (Fig. 1), are not associated with many coherent, statistically significant SST anomalies. Further
357 investigation using longer observational records and focusing on different seasons is needed to
358 better understand the predictability—or lack thereof—of tornado activity.

Composite SST Anomalies by WR Phases



359

360 **Figure 7:** April SST anomalies for active and inactive WR years, and hatching indicates significant SST anomalies
361 ($p \leq 0.05$) using a one-sample, two-sided t-test. 500h anomalies are shown in black contours.



362

363 4. Summary

364 A hybrid model for the seasonal prediction of CONUS springtime tornado activity is evaluated
365 during 1981-2023. The model employs WR forecasts from the ECMWF ensemble springtime
366 forecasts initialized on April-1st. Using the leave-one-year-out cross-validation, the WR-based
367 model shows no predictive skill for TDs, but the predicted time series of TO days is significantly
368 correlated with the observed time series. Predictive skill for TOs is modulated by low-frequency
369 climate modes and is significantly enhanced during +AO, +NAO, +PNA, and El Niño years, with
370 the proportion correct of 75%, 71.4%, 71.4%, and 70%, respectively. Given the difficulty of
371 predicting TDs beyond subseasonal timescales (Gensini et al. 2020), springtime prediction efforts
372 should prioritize TOs due to their higher predictive skill and societal impacts, and low-frequency
373 climate modes can help to identify forecasts of opportunity.

374 To investigate the predictability sources of springtime tornado activity, the composite TD and TO
375 probability anomalies were examined during different phases of climate modes. Significantly
376 enhanced TO probability anomalies were associated with -AO and La Niña years, while
377 significantly reduced TO probability anomalies were associated +NAO and +PNA years.
378 Corresponding circulation patterns during these years provide physical support, through CAPE
379 and vertical shear anomalies. TO probability anomalies are generally stronger than TD anomalies
380 associated with climate modes, which helps explain the higher predictive skill of TOs.

381 Additionally, WR occurrence is modulated by some climate modes. WR-A is the dominant WR
382 during +NAO years and WR-E is the dominant WR during +PNA years, consistent with reduced
383 tornado activity during +NAO and +PNA years. Furthermore, WR-B is the dominant WR during
384 -AO years and is the least frequent WR during +PNA years, consistent with enhanced (reduced)
385 tornado activity during the -AO (+PNA) phase. WRs associated with increased springtime tornado
386 activity tend to occur more frequently during the climate mode phases that favor increased tornado
387 activity, while WRs associated with suppressed tornado activity preferentially occur during
388 climate mode phases that are unfavorable for tornado activity. This physical consistency supports
389 the use of WRs as a physically meaningful framework for predicting TOs.

390 The role of SSTs in the predictability of WRs (with implication for the predictability of tornado
391 activity) was examined, with the focus on April SST anomalies. -WR-A years feature a -NAO SST
392 and 500H pattern over the North Atlantic, consistent with WR-A being suppressed during -NAO
393 patterns. +WR-B years feature positive, though insignificant, SSTs over the central Pacific
394 consistent with patterns shown in Chu et al. (2019) for April tornadoes. In addition, significantly
395 negative SST anomalies exist over the northern Pacific during -WR-B years, consistent with
396 suppressed WR-B and TO during +PNA years. Overall, SST anomalies can help explain WR
397 predictability, but SST signals for some WRs are insignificant or patchy, making it challenging to
398 identify specific SST-based predictors for WRs or tornado activity. Further investigation based on
399 longer observational records would help better understand the role of SST in the predictability of
400 WRs and tornado activity.

401 This study demonstrates that skillful prediction of springtime TOs is indeed possible with current
402 resources via the connection between tornado activity and WRs. Questions remain on whether
403 SSTs are a reliable driver of springtime TOs as well as the temporal extent to which TOs can be
404 predicted.

405



406 **Code Availability**

407 Important python files for WR identification and modeling are included at the following link:

408 <https://github.com/Matt0604/Springtime-Prediction-Manuscript>

409

410 **Data Availability**

411 The ERA5 data are available through the NCAR research data archive (RDA) (d633000) and the
412 Copernicus Climate Data Store (CDS):

413 <https://doi.org/10.24381/cds.bd0915c6> (Hersbach et al. 2023a)

414 <https://doi.org/10.24381/cds.adbb2d47>(Hersbach et al. 2023b)

415 The ECMWF data are available through the Copernicus Climate Data Store (CDS):

416 <https://doi.org/10.24381/cds.50ed0a73> (Copernicus Climate Change Service 2018)

417 April SST data are available through the Extended-range sea surface temperatures data (Huang et
418 al. 2017).

419 The tornado report data used in this study are available through the NOAA Storm Prediction Center
420 severe weather database:

421 <https://www.spc.noaa.gov/wcm/#data>

422

423 **Author Contributions**

424 Conceptualization: MG, ZW, RJT

425 Methodology: MG, ZW, RJT

426 Project Administration: ZW, RJT

427 Supervision: ZW, RJT

428 Writing – Original Draft: MG

429 Writing – Review and Edits: MG, ZW, RJT

430

431 **Competing Interests**

432 Authors declare they have no competing interest.

433

434 **Acknowledgements**

435 We acknowledge the NCAR Computation and Information Systems Laboratory (CISL) for
436 providing computing resources through Derecho. All ERA5 data used in this study are available
437 at the research data archive. All ECMWF seasonal forecast data are available via the Copernicus
438 Climate Change Service. Tornado report data are available through the NOAA Storm Prediction
439 Center severe weather database.

440



441 **References**

- 442 Allen, J. T., M. K. Tippett, and A. H. Sobel, 2015: Influence of the El Niño/Southern Oscillation on tornado
443 and hail frequency in the United States. *Nat. Geosci.*, **8**, 278–283,
444 <https://doi.org/10.1038/ngeo2385>.
- 445 —, M. J. Molina, and V. A. Gensini, 2018: Modulation of annual cycle of tornadoes by El-Niño-
446 Southern Oscillation. *Geophys. Res. Lett.*, **45**, 5708–5717,
447 <https://doi.org/10.1029/2018GL077482>.
- 448 Ashley, W. S., 2007: Spatial and temporal analysis of tornado fatalities in the United States: 1880–2005.
449 *Weather Forecast.*, **22**, 1214–1228, <https://doi.org/10.1175/2007WAF2007004.1>.
- 450 Brooks, H. E., G. W. Carbin, and P. T. Marsh, 2014: Increased variability of tornado occurrence in the
451 United States. *Science*, **346**, 349–352, <https://doi.org/10.1126/science.1257460>.
- 452 Charney, J. G., and J. G. DeVore, 1979: Multiple flow equilibria in the atmosphere and blocking. *J.*
453 *Atmospheric Sci.*, **36**, 1205–1216, [https://doi.org/10.1175/1520-](https://doi.org/10.1175/1520-0469(1979)036%3C1205:MFEITA%3E2.O.CO;2)
454 [0469\(1979\)036%3C1205:MFEITA%3E2.O.CO;2](https://doi.org/10.1175/1520-0469(1979)036%3C1205:MFEITA%3E2.O.CO;2).
- 455 Childs, S., R. S. Schumacher, and J. T. Allen, 2018: Cold-season tornadoes: Climatological and
456 meteorological insights. *Weather Forecast.*, **33**, 671–691, [https://doi.org/10.1175/WAF-D-17-](https://doi.org/10.1175/WAF-D-17-0120.1)
457 [0120.1](https://doi.org/10.1175/WAF-D-17-0120.1).
- 458 Chu, J.-E., A. Timmermann, and J.-Y. Lee, 2019: North American April tornado occurrences linked to
459 global sea surface temperature anomalies. *Sci. Adv.*, **5**, <https://doi.org/10.1126/sciadv.aaw9950>.
- 460 Cook, A. R., and J. T. Schaefer, 2008: The relation of El Niño-Southern Oscillation (ENSO) to winter
461 tornado outbreaks. *Mon. Weather Rev.*, **136**, 3121–3137,
462 <https://doi.org/10.1175/2007MWR2171.1>.
- 463 —, L. Leslie, D. Parsons, and J. Schaefer, 2017: The impact of El Niño-Southern Oscillation (ENSO) on
464 Winter and early Spring U.S. tornado outbreaks. *J. Appl. Meteorol. Climatol.*, **56**, 2455–2478,
465 <https://doi.org/10.1175/JAMC-D-16-0249.1>.
- 466 Copernicus Climate Change Service, C. D. S., 2018: Seasonal forecast subdaily data on pressure levels.
467 Copernicus Climate Change Service (C3S) Climate Data Store (CDS), accessed 1 June 2025,
468 <https://doi.org/10.24381/cds.50ed0a73>.
- 469 Cwik, P., R. A. McPherson, M. B. Richman, and A. E. Mercer, 2022: Climatology of 500-hPa geopotential
470 height anomalies associated with May tornado outbreaks in the United States. *Int. J. Climatol.*,
471 **43**, 893–913, <https://doi.org/10.1002/joc.7841>.
- 472 Czaja, A., and C. Frankignoul, 2002: Observed Impact of Atlantic SST Anomalies on the North Atlantic
473 Oscillation. *J. Clim.*, **15**, 606–623, [https://doi.org/10.1175/1520-](https://doi.org/10.1175/1520-0442(2002)015%3C0606:OIOASA%3E2.O.CO;2)
474 [0442\(2002\)015%3C0606:OIOASA%3E2.O.CO;2](https://doi.org/10.1175/1520-0442(2002)015%3C0606:OIOASA%3E2.O.CO;2).
- 475 Duan, W., and C. Wei, 2012: The ‘spring predictability barrier’ for ENSO predictions and its possible
476 mechanism: Results from a fully coupled model. *Int. J. Climatol.*, **33**, 1280–1292.



- 477 Elsner, J. B., T. H. Jagger, and T. Fricker, 2016: Statistical models for tornado climatology: Long and short-
478 term views. *PLoS ONE*, **11**, <https://doi.org/10.1371/journal.pone.0166895>.
- 479 Gensini, V. A., and M. K. Tippett, 2019: Global Ensemble Forecast System (GEFS) predictions of days 1-15
480 U.S. tornado and hail frequencies. *Geophys. Res. Lett.*, **46**, 2922–2930,
481 <https://doi.org/10.1029/2018GL081724>.
- 482 —, B. S. Barrett, J. T. Allen, D. Gold, and P. Sirvatka, 2020: The Extended-Range Tornado Activity
483 Forecast (ERTAF) Project. *Bull. Am. Meteorol. Soc.*, **101**, E700–E709,
484 <https://doi.org/10.1175/BAMS-D-19-0188.1>.
- 485 Graber, M., R. J. Trapp, and Z. Wang, 2024: The regionality and seasonality of tornado trends in the
486 United States. *Npj Clim. Atmospheric Sci.*, **7**, <https://doi.org/10.1038/s41612-024-00698-y>.
- 487 —, Z. Wang, and R. J. Trapp, 2025: Linking weather regimes to the variability of warm-season tornado
488 activity over the United States. *Weather Clim. Dyn.*, **6**, 807–816, <https://doi.org/10.5194/wcd-6-807-2025>.
- 490 Hannachi, A., D. M. Straus, C. L. E. Franzke, S. Corti, and T. Woollings, 2017: Low-frequency nonlinearity
491 and regime behavior in the northern hemisphere extratropical atmosphere. *Rev. Geophys.*, **55**,
492 199–234, <https://doi.org/10.1002/2015RG000509>.
- 493 Hersbach, H., and Coauthors, 2020: The ERA5 global reanalysis. *Q. J. R. Meteorol. Soc.*, **146**, 1999–2049,
494 <https://doi.org/10.1002/qj.3803>.
- 495 —, and Coauthors, 2023a: ERA5 hourly data on pressure levels from 1940 to present. Copernicus
496 Climate Change Service (C3S) Climate Data Store (CDS), accessed 1 October 2025,
497 <https://doi.org/10.24381/cds.bd0915c6>.
- 498 —, and Coauthors, 2023b: ERA5 hourly data on single levels from 1940 to present. Copernicus Climate
499 Change Service (C3S) Climate Data Store (CDS), accessed 1 October 2025,
500 <https://doi.org/10.24381/cds.adbb2d47>.
- 501 Huang, B., and Coauthors, 2017: Extended Reconstructed Sea Surface Temperature, version 5 (ERSSTv5):
502 Upgrades, validations, and intercomparisons. *15 Oct 2017*, **30**, 8179–8205,
503 <https://doi.org/10.1175/JCLI-D-16-0836.1>.
- 504 Jiang, Q., D. T. Dawson II, L. Funing, and D. R. Chavas, 2025: Classifying synoptic patterns driving tornadic
505 storms and associated spatial trends in the United States. *Npj Clim. Atmospheric Sci.*, **8**,
506 <https://doi.org/10.1038/s41612-025-00897-1>.
- 507 Lee, S. H., M. K. Tippett, and L. M. Polvani, 2023: A new year-round weather regime classification for
508 North America. *J. Clim.*, **36**, 7091–7108, <https://doi.org/10.1175/JCLI-D-23-0214.1>.
- 509 Lee, S.-K., A. T. Wittenberg, D. B. Enfield, S. J. Weaver, C. Wang, and R. Atlas, 2016: US regional tornado
510 outbreaks and their links to spring ENSO phases and North Atlantic SST variability. *Environ. Res.
511 Lett.*, **11**, <https://doi.org/10.1088/1748-9326/11/4/044008>.



- 512 Lepore, C., M. K. Tippett, and J. T. Allen, 2017: ENSO-based probabilistic forecasts of March-May U.S.
513 tornado and hail activity. *Geophys. Res. Lett.*, **44**, 9093–9101,
514 <https://doi.org/10.1002/2017GL074781>.
- 515 Mercer, A. E., C. M. Shafer, C. A. Doswell III, L. M. Leslie, and M. B. Richman, 2012: Synoptic composites
516 of tornadic and nontornadic outbreaks. *Mon. Weather Rev.*, **140**, 2590–2608,
517 <https://doi.org/10.1175/MWR-D-12-00029.1>.
- 518 Michelangeli, P.-A., R. Vautard, and B. Legras, 1995: Weather regimes: Recurrence and quasi
519 stationarity. *J. Atmospheric Sci.*, **52**, 1237–1256, [https://doi.org/10.1175/1520-0469\(1995\)052%3C1237:WRRASQ%3E2.0.CO;2](https://doi.org/10.1175/1520-0469(1995)052%3C1237:WRRASQ%3E2.0.CO;2).
- 521 Miller, D., Z. Wang, R. J. Trapp, and D. S. Harnos, 2020: Hybrid prediction of weekly tornado activity out
522 to week 3: Utilizing weather regimes. *Geophys. Res. Lett.*, **47**,
523 <https://doi.org/10.1029/2020GL087253>.
- 524 Molina, M. J., R. P. Timmer, and J. T. Allen, 2016: Importance of the Gulf of Mexico as a climate driver for
525 U.S. severe thunderstorm activity. *Geophys. Res. Lett.*, **43**, 12295–12304,
526 <https://doi.org/10.1002/2016GL071603>.
- 527 Moore, T. W., 2018: Annual and seasonal tornado trends in the Contiguous United States and its regions.
528 *Int. J. Climatol.*, **38**, 1582–1594, <https://doi.org/10.1002/joc.5285>.
- 529 —, 2019: Seasonal frequency and spatial distribution of tornadoes in the United States and their
530 relationship to the El Niño/Southern Oscillation. *Ann. Am. Assoc. Geogr.*, **109**, 1033–1051,
531 <https://doi.org/10.1080/24694452.2018.1511412>.
- 532 Munoz, E., and D. Enfield, 2011: The boreal spring variability of the Intra-Americas low-level jet and its
533 relation with precipitation and tornadoes in the eastern United States. *Clim. Dyn.*, **36**, 247–259.
- 534 National Weather Service, 2025: 80-year list of severe weather fatalities.
- 535 NCEI, 2024: U.S. billion-dollar weather and climate disasters.
- 536 Niloufar, N., N. Devineni, V. Were, and R. Khanbilvardi, 2021: Explaining the trends and variability in the
537 United States tornado records using climate teleconnections and shifts in observational
538 practices. *Sci. Rep.*, **11**, <https://doi.org/10.1038/s41598-021-81143-5>.
- 539 NOAA Climate Prediction Center, 2024a: Oceanic Niño Index (ONI) v5 - Monthly SST anomalies in the
540 Niño 3.4 region, accessed 1 September 2025,
541 https://www.cpc.ncep.noaa.gov/products/analysis_monitoring/ensostuff/ONI_v5.php.
- 542 —, 2024b: Daily climate mode indices, accessed 1 September 2025,
543 <https://ftp.cpc.ncep.noaa.gov/cwlinks/>.
- 544 Schneider, R. S., J. T. Schaefer, and H. E. Brooks, 2004: Tornado outbreak days: An updated and
545 expanded climatology (1875–2003). Vol. P5.1 of, 22nd Conference on Severe Local Storms,
546 Hyannis, MA, American Meteorological Society.



- 547 Sherburn, K. D., M. D. Parker, J. R. King, and G. Lackmann, 2016: Composite environments of severe and
548 nonsevere high-shear, low-CAPE convective events. *Weather Forecast.*, **31**, 1899–1927,
549 <https://doi.org/10.1175/WAF-D-16-0086.1>.
- 550 Strader, S. M., V. A. Gensini, W. S. Ashley, and A. N. Wagner, 2024: Changes in tornado risk and societal
551 vulnerability leading to greater tornado impact potential. *Npj Nat. Hazards*, **1**,
552 <https://doi.org/10.1038/s44304-024-00019-6>.
- 553 Tippet, M. K., C. Lepore, and M. L. L’Heureux, 2022: Predictability of a tornado environment index from
554 El Nino Southern Oscillation (ENSO) and the Arctic Oscillation. *Weather Clim. Dyn.*, **3**, 1063–
555 1075, <https://doi.org/10.5194/wcd-3-1063-2022>.
- 556 —, K. Malloy, and S. H. Lee, 2024: Modulation of U.S. tornado activity by year-round North American
557 weather regimes. *Mon. Weather Rev.*, **152**, 2189–2202, <https://doi.org/10.1175/MWR-D-24-0016.1>.
558
- 559 Trapp, R. J., 2013: *Mesoscale-convective processes in the atmosphere*. Cambridge University Press.
- 560 —, 2014: On the significance of multiple consecutive days of tornado activity. *Mon. Weather Rev.*,
561 **142**, 1452–1459, <https://doi.org/10.1175/MWR-D-13-00347.1>.
- 562 Vitart, F., and Coauthors, 2017: The subseasonal to seasonal (S2S) prediction project database. *Bull. Am.*
563 *Meteorol. Soc.*, **98**, 163–173, <https://doi.org/10.1175/BAMS-D-16-0017.1>.
- 564 Zhang, W., S. S-Y Wang, Y. Chikamoto, R. Gillies, M. LaPlante, and V. Hari, 2024: A weather pattern
565 responsible for increasing wildfires in the western United States. *Environ. Res. Lett.*, **20**,
566 <https://doi.org/10.1088/1748-9326/ad928f>.
- 567 Zhao, J., L. Bai, B. Zhou, and L. Zhang, 2025: Contributions of Interdecadal Pacific Oscillation, Atlantic
568 Multidecadal Oscillation, and global ocean warming to the secular change in United States
569 tornado occurrence. *Atmospheric Res.*, **331**, <https://doi.org/10.1016/j.atmosres.2025.108689>.
- 570
- 571